**Atmospheric
Measurement
Techniques**
Open Access

Discussions

Water vapor retrieval from OMI visible spectra

H. Wang[1], X. Liu[1], K. Chance[1], G. Gonzalez Abad[1], and C. Chan Miller[2]

[1]Harvard-Smithsonian Center for Astrophysics, Cambridge, MA 02138, USA
[2]Department of Earth and Planetary Sciences, Harvard University, Cambridge, MA 02138, USA

Correspondence to: H. Wang (hwang@cfa.harvard.edu)

Discussion Paper | Discussion Paper | Discussion Paper | Discussion Paper |

AMTD

7, 541–567, 2014

Water vapor retrieval from OMI visible spectra

H. Wang et al.

Title Page

Abstract	Introduction
Conclusions	References
Tables	Figures

|◄ | ►|

◄ | ►

Back | Close

Full Screen / Esc

Printer-friendly Version

Interactive Discussion

Abstract

There are distinct spectral features of water vapor in the wavelength range covered by the Ozone Monitoring Instrument (OMI) visible channel. Although these features are much weaker than those at longer wavelengths, they can be exploited to retrieve useful information about water vapor. They have an advantage in that their small optical depth leads to fairly simple interpretation as measurements of the total water vapor column density. We have used the Smithsonian Astrophysical Observatory (SAO)'s OMI operational retrieval algorithm to derive the Slant Column Density (SCD) of water vapor from OMI measurements using the 430–480 nm spectral region after extensive optimization of retrieval windows and parameters. The Air Mass Factor (AMF) is calculated using look-up tables of scattering weights and monthly mean water vapor profiles from the GEOS-5 assimilation products. We convert from SCD to Vertical Column Density (VCD) using the AMF and generate associated retrieval averaging kernels and shape factors. Our standard water vapor product has a median SCD of $\sim 1.3 \times 10^{23}$ molecule cm^{-2} and a median relative uncertainty of $\sim 11\%$ in the tropics, about a factor of 2 better than that from a similar OMI algorithm but using narrower retrieval window. The corresponding median VCD is $\sim 1.2 \times 10^{23}$ molecule cm^{-2}. We have also explored the sensitivities to various parameters and compared our results with those from the Moderate-resolution Imaging Spectroradiometer (MODIS) and the Aerosol Robotic NETwork (AERONET).

1 Introduction

Water vapor is one of the key factors for weather. It is also the most abundant greenhouse gas in the atmosphere. It can provide strong feedback directly through amplification of global warming associated with other greenhouse gases and indirectly through formation of clouds. Water vapor participates in many photochemical reactions, such as the reaction with $O(^1D)$ to produce OH radical which controls the oxidation capacity

of the atmosphere. It is therefore also important for atmospheric chemistry. Unlike other long-lived greenhouse gases, the short-lived water vapor exhibits large spatial and temporal variability. Monitoring the distribution, variability and long-term changes in water vapor is critical for understanding the hydrological cycle, the Earth radiative budget and

5   climate change.

Water vapor has long been observed using a variety of platforms and methods, including measurements made from surface stations, balloons, aircrafts and satellites using in-situ or remote sensing techniques. Satellite observations of water vapor have used microwave (e.g., Advanced Microwave Sounding Unit (AMSU), Advanced Mi-

10 crowave Scanning Radiometer-Earth Observing System (AMSR-E), Special Sensor Microwave/Imager (SSM/I), Special Sensor Microwave Imager/Sounder (SSMI/S); Ferraro et al., 2005; Boukabara et al., 2010), thermal infrared (e.g., Moderate Resolution Imaging Spectrometer (MODIS) (King et al., 2003), Tropospheric Emission Spectrometer (TES) (Worden et al., 2012), Atmospheric Infrared Sounder (AIRS) (Aumann

15 et al., 2003), Infrared Atmospheric Sounding Interferometer (IASI) (Schneider and Hase, 2011)), and near infrared and visible (e.g., MODIS (King et al., 2003), Global Ozone Monitoring Experiment (GOME) (Noel et al., 2002; Wagner et al., 2003), Scanning Imaging Absorption spectrometer for Atmospheric CHartographY (SCIAMACHY) (Noel et al., 2004)) sensors.

20 Wagner et al. (2013) demonstrated the feasibility of water vapor retrieval in the blue spectral range using GOME-2 and OMI measurements. They pointed out that the advantages for this spectral range include more consistent retrievals across the globe due to more uniform surface albedo, especially between land and ocean, increased sensitivity to near surface layer due to higher surface albedo over the oceans than for longer

25 wavelengths, less saturation of signal due to weaker water vapor absorption, applicability to sensors that do not cover longer wavelengths, and daily global coverage over a long period of time.

Wagner et al. (2013) derived OMI water vapor SCDs. We have independently derived water vapor SCDs and converted them to vertical column density (VCD) from OMI

Water vapor retrieval from OMI visible spectra

H. Wang et al.

visible spectra using the Smithsonian Astrophysical Observatory (SAO) operational retrieval algorithm after optimization of the fitting window and parameters. In this paper, we will present our SCD retrievals, vertical VCD calculations, sensitivity studies and validation results.

2   Data processing

2.1   OMI instrument and OMI data

OMI is a joint Dutch-Finnish instrument onboard the NASA EOS-Aura satellite which was launched on 15 July 2004 into a sun-synchronous orbit with an ascending node equator crossing time around 1:45 p.m. and an orbital period of about 100 min (Schoeberl et al., 2006). It is a nadir-viewing push-broom Ultraviolet/Visible (UV/VIS) imaging spectrometer with three channels – the UV1 (264–311 nm), UV2 (307–383 nm) and VIS (349–504 nm) – at 0.42–0.63 nm spectral resolution (Levelt et al., 2006). For the visible channel, the 2600 km OMI cross-track swath usually provides a nominal spatial resolution between 13 km × 24 km at nadir and 26 km× ∼ 135 km at the edge. The entire globe is covered by 14–15 orbits each day. Solar irradiance measurements are performed daily.

We use Version 3 Level 1B OMI visible spectra to derive water vapor SCD, and Version 003 Level-2 OMI cloud pressure and cloud fraction product (OMCLDO2) downloaded from disc.sci.gsfc.gov/Aura/data-holdings/OMI/ for AMF calculation. The cloud information is derived using the O_2–O_2 absorption band at ∼ 477 nm (Stammes and Noordhoek, 2002; Acaretta et., 2004).

2.2 Slant column retrieval

2.2.1 Standard retrieval

We determine the slant column of water vapor by directly fitting the OMI spectra following the method described in Chance (1998). The method is also presented in detail in Gonzalez Abad et al. (2014). In this paper, we only provide a brief description.

Wavelength calibration is performed using cross correlation through spectral shift (Caspar and Chance, 1997) with a high-resolution solar reference spectrum (Chance and Kurucz, 2010). To reduce noise, we use the leading principle component derived from OMI solar spectra as the measured solar spectrum. The slant column abundance that minimizes the difference between the measured and calculated radiance is retrieved using a non-linear least squares inversion method by Lindström and Wedin (1988). We use a spectral window from 430 nm to 480 nm for our standard water vapor retrieval. A 3rd order polynomial is fitted for both the baseline and the scaling factor to account for broadband spectral features. Common mode and under-sampling spectra (Chance et al., 2005) are derived on-line and applied to the fitting. The retrieval takes into consideration water vapor, ozone, nitrogen dioxide, oxygen collision complex, liquid water, glyoxal, the Ring effect (Chance and Spurr, 1997) and the liquid water Ring effect. The molecular reference spectra used in our standard retrieval are listed in Table 1 and plotted in Fig. 1. There are distinct spectral signatures of these molecules in our retrieval window. The reference spectra are interpolated onto common calibrated radiance grid and convolved with pre-determined instrument slit function (Dirksen et al., 2006) during the fitting (Fig. 1). Ozone, nitrogen dioxide, water vapor and glyoxal are corrected for the solar I_0 effect (Aliwell et al., 2002).

Figure 2 shows our standard retrieval result for the SCD and the associated absolute and relative uncertainties for 14 July 2005 (orbits 5297–5311). As expected, the global pattern shows more water vapor in the Intertropical Convergence Zone (ITCZ) and mid-latitude weather systems. There are some stripes along the swaths (Veihelmann and Kleipool, 2006) as we have not applied our post-processing de-stripping

routine for this plot. The stripes are mainly caused by OMI systematic measurement errors and are common to most OMI level 2 products. In the tropics (30° S–30° N), the median of SCD is 1.32×10^{23} molecules cm^{-2}, the median of fitting uncertainty is 1.2×10^{22} molecules cm^{-2}, the median of relative uncertainty (fitting uncertainty/SCD)

5 is 11 % and the median of fitting Root Mean Squared (RMS) is 9.2×10^{-4}. Areas with larger SCD generally have smaller uncertainties.

The 25 % and 75 % percentiles of our fitting uncertainties in the tropics are 1.0×10^{22} and 1.7×10^{22} molecules cm^{-2}, respectively. In comparison, using a shorter retrieval window of 430–450 nm, Wagner et al. (2013) obtained typical SCD uncertainties

10 of 3–5×10^{22} molecules cm^{-2} for OMI and 1–2.5×10^{22} molecules cm^{-2} for GOME-2. The uncertainty of our standard water vapor SCD is therefore smaller than Wagner et al. (2013)'s OMI result and similar to Wagner et al. (2013)'s GOME-2 result.

Figure 3 shows examples of our spectral fitting for two pixels from orbit 5306 in July 2005. The left column is for a pixel at 1.75° S and 34.6° W in the Atlantic

15 ocean, and the right column is for a pixel at 47.75° N and 53.4° W at the Atlantic coast of North America. The retrieved water vapor SCDs are $(1.23 \pm 0.12) \times 10^{23}$ and $(1.75 \pm 0.07) \times 10^{23}$ molecules cm^{-2}, respectively, close to the median SCD for the orbit. The corresponding RMS values are 1.1×10^{-3} and 4.0×10^{-4}, respectively. The panels in the top row show that the fitted spectra (red) closely track the measured

20 spectra (black). The panels in the second row show that the fitting residuals appear random. The next four rows show the reference spectra of important molecules (water vapor, liquid water, nitrogen dioxide and ozone) scaled by their corresponding fitted SCDs (black) and added to the fitting residuals in the second row (red). In both cases, the water vapor spectral signature within the fitting window is stronger than the fitting

25 residuals. Consistent with the expectation that there is less liquid water, more NO_2 and more O_3 in the mid-latitude coastal area than in the tropical open ocean, the right panels show that the liquid water signal is weaker and the NO_2 and O_3 signals are stronger than the residual, while the left panels show the opposite.

Water vapor retrieval from OMI visible spectra

H. Wang et al.

Title Page

Abstract   Introduction

Conclusions   References

Tables   Figures

◄   ►

◄   ►

Back   Close

Full Screen / Esc

Printer-friendly Version

Interactive Discussion

2.2.2 Sensitivity studies

We investigate the sensitivity of OMI water vapor SCD with respect to the retrieval window. Selected examples are listed in Table 2. We vary the retrieval window while keeping everything else the same. All the retrieval windows in Table 2 include the water vapor feature at $\sim$ 442 nm. The 438–478 nm and the standard 430–480 nm window also include the weaker water vapor feature at $\sim$ 470 nm, and the longest window (430–495 nm) includes an additional weaker feature at $\sim$ 485 nm. The median SCDs and uncertainties within 30° N–30° S on 14 July 2005 are listed in Table 2. The standard window leads to the smallest uncertainty (1.2×10^{22} molecules cm^{-2}). The uncertainties for the 20 nm and 30 nm windows are about 100 % and 60 % larger, respectively. The uncertainty for the 65 nm window is about 25 % larger. The median SCD decreases from 1.47×10^{23} to 1.23×10^{23} molecules cm^{-2} as the retrieval window length increases.

We have performed additional sensitivity studies, shown in Table 3, by excluding the interfering molecules, changing the reference spectra and changing the order of closure polynomials. In these experiments, everything else is kept the same as in the standard retrieval. We list the median statistics and the number of negative retrievals for water vapor between 30° S and 30° N for 14 July 2005 in Table 3.

Exclusion of O_3, O_2–O_2, NO_2 or liquid water leads to significant (10–30 %) reduction of the retrieved water vapor SCDs and large increase of the number of negative retrievals, though the fitting uncertainties and RMS remain at the same level. The most severe change is associated with liquid water, followed by NO_2, O_2–O_2 and O_3. Exclusion of $C_2H_2O_2$ leads to only a $\sim$ 1 % increase of water vapor SCD. Without liquid water, the medium water vapor SCD decreases by $\sim$ 32 % from 1.32×10^{23} to 0.90×10^{23} molecules cm^{-2} and the number of negative retrievals increases from 1935 to 50 216. As a by-product of our standard water vapor retrieval, the top panel of Fig. 4 shows the retrieved liquid water. Although the retrieval is not optimized for liquid water, areas in the oceans, seas, gulfs and so on are highlighted. Not all liquid water bodies are highlighted to the same extent. Comparison between the top and middle panels of

Fig. 4 shows that some liquid water surfaces are shielded by cloud cover. The bottom panel of Fig. 4 shows the retrieved water vapor SCD without considering liquid water. Compared to the standard retrieval in the top panel of Fig. 2, the SCDs here are apparently smaller, especially over the areas with liquid water where lots of negative values (plotted as blanks) are retrieved. It should be noted that such a strong sensitivity to liquid water is for the standard long retrieval window of 430–480 nm. For the shorter window of 432–462 nm, the difference in median SCD with and without liquid water is only $\sim 4\%$ which is substantially smaller than the median relative uncertainty.

Switching from HITRAN 2008 (Rothman et al., 2009) to HITRAN 2012 (Rothman et al., 2013) water vapor reference makes the median SCD about 6 % lower than that of the standard retrieval. In comparison, the median relative uncertainty of the standard retrieval is $\sim 11\%$. Switching to the Thalman et al. (2013) O_2–O_2 reference spectrum gives almost the same result as the standard retrieval, so does switching from a 3rd order to a 5th order polynomial for the baseline and scaling factor. The median of SCD retrieved using water vapor reference spectrum at 0.7 atm and 265 K is $\sim 2\%$ lower than the standard result, and that using water vapor reference at 1.0 atm and 288 K is $\sim 2\%$ higher.

3 Vertical column calculation

To derive the vertical column density (VCD), we divide the SCD by the Air Mass Factor (AMF), i.e., VCD = SCD/AMF. The AMF is defined as the vertical integral of the product of the scattering weight and the shape factor, where the scattering weight accounts for the sensitivity of the measurement to water vapor as a function of altitude and the shape factor accounts for the normalized vertical profile of water vapor (Palmer et al., 2001). Detailed description of AMF calculation for our operational retrieval algorithm can be found in Gonzalez Abad et al. (2014). Averaging kernels can be derived as the ratio of scattering weights to AMF (Eskes and Boersma, 2003) and are provided in our

level 2 products together with the H_2O shape factor for comparison with or assimilation into models.

The a priori vertical profiles of water vapor are from the monthly mean GEOS-5 data assimilation product. They are generated at the Global Modeling and Assimilation Office (GMAO) and re-gridded to $2°$ latitude $\times 2.5°$ longitude $\times 47$ layer resolution for GEOS-Chem simulations.

The scattering weights are calculated using the VLIDORT radiative transfer model (Spurr, 2006). Due to very weak wavelength dependence of the scattering weight in our retrieval window (Gonzalez Abad et al., 2014), we choose to use the one at $\lambda = 442\,nm$ in our operational retrieval. Using the average of the whole retrieval window ($[430, 480]\,nm$) results in less than $\sim 1\%$ of a difference in the VCDs. To speed up the computation, we prepare a scattering weight look-up table based on the surface albedo, observational geometry, height above the surface and height at cloud top. For partly cloudy scenes, the scattering weight is approximated as the radiative cloud fraction weighted average of the clear and cloudy part (Martin et al., 2002). We use the cloud fraction and cloud top pressure from the Version 3 Level-2 OMICLDO2 product which is derived using the O_2–O_2 absorption band at $\sim 477\,nm$ (Acaretta et al., 2004). The error associated with the AMFs are most likely larger than the error associated with water vapor SCDs. Detailed analysis of the AMF error will be performed later. Examples of VCD maps are shown in the top panels of Fig. 5 and will be discussed in the next section.

4 Validation

In this section, we compare our VCDs with those derived from MODIS near-IR data and AERONET ground-based measurements.

The MODIS near-IR total precipitable water product (Gao and Kaufman, 2003) is derived using the ratios of water vapor absorbing channels (0.905, 0.936 and 0.94 μm) and atmospheric window channels (0.865 and 1.24 μm) in the near-IR. The retrieval

algorithm relies on observations of water vapor attenuation of reflected solar radiation, therefore results only exist for reflective surfaces in the near-IR. The errors are typically about 5–10 %, with greater errors over dark surfaces and under hazy conditions. In this paper, we use MODIS Level-3 monthly $1° × 1°$ data (MYD08_M3) collected from the Aqua platform which observes at 1:45 p.m. (ladsweb.nascom.nasa.gov/data/).

The top panels of Fig. 5 show our results of the monthly mean $1° × 1°$ water vapor VCDs derived from the standard OMI water vapor retrieval for January and July 2006. For easy comparison with the MODIS products, we have converted the VCDs from molecules cm^{-2} to precipitable cm using a multiplication factor of $2.98904 × 10^{-23}$. The $1° × 1°$ VCDs are calculated using the weighted average of the retrieved VCDs whose cloud fractions are less than 0.25. The weight for the retrieval is assigned according to both the area of the ground pixel within the grid box and the fitting uncertainty. The number of data points for a grid box ranges from 0 to ~ 900 with a median of ~ 100. Stripes in daily maps (Fig. 2) are averaged out in the monthly maps.

For comparison, the corresponding MODIS maps are shown in the panels on the second row of Fig. 5. There are more missing data (blank areas) in MODIS than in OMI maps due to the low near-IR surface reflectivity over the ocean. Both OMI and MODIS results show the seasonal shift of the ITCZ. The OMI – MODIS difference panels are shown on the next row. The bottom panels show the scatter plots of MODIS vs. OMI results. There is a general linear relationship between them for both January and July, with a linear correlation coefficient of 0.92 and 0.89, respectively. The regression lines are indicated in the plot. In January 2006, the mean of OMI has a negative bias of 0.25 cm compared to MODIS, and the standard deviation of the difference is 0.62 cm. However, for OMI precipitable water > 3 cm, the mean of OMI is higher than that of MODIS by 0.19 cm. This is consistent with the redder tone in the tropics shown by the difference maps, and is probably related to the higher surface reflectivity over the ocean in the UV than in the near IR. In July 2006, the data points are better clustered around the 1 : 1 line. The difference of OMI – MODIS has a mean of -0.07 cm and a standard

deviation of 0.62 cm. Again, for OMI > 3 cm, the mean of OMI is higher than that of MODIS by 0.26 cm.

AERONET is a network of globally distributed ground-based visible and near-IR sun photometers that measure atmospheric aerosol properties, inversion products, and precipitable water (aeronet.gsfc.nasa.gov) (Holben et al., 1998). Total water vapor column is retrieved from the 935 nm channel. The data used in this study are Version 2 daily averages. They are pre- and post-field calibrated, automatically cloud cleared and manually inspected.

Figure 6 shows the scatter plots of nearly coincident OMI and AERONET precipitable water for January and July in 2005 and 2006. All valid AERONET observations for the month are included for each panel. To find the nearly coincident observations, we use OMI retrievals that have cloud fraction of < 0.25 and are within a 0.5° radius of the AERONET site on the same day. There are typically 1–6 OMI data points for each AERONET data point, and they are averaged for comparison. Since artificial stripes in OMI swaths (Fig. 2) can significantly influence the comparison in this case, we post-process OMI VCDs to remove the stripes by dividing a normalization vector. The normalization vector is derived using the mean of the middle third of the monthly averaged swaths and normalized so that the mean of the vector is unity.

The majority of data in Fig. 6 exhibit linear relationship between AERONET and OMI observations. There appears to be better agreement in January than in July for both years. The slopes of the AERONET vs. OMI regression lines are < 1. Considering that coincident OMI results have much larger uncertainty here than in Fig. 5 due to far less number of data points available for averaging, in addition to the different observational footprint and the highly variable nature of water vapor, the degree of agreement indicates that water vapor retrieval using OMI spectra is very promising.

Figure 7 shows time series comparisons between daily AERONET and OMI precipitable water for selected sites. This figure shows comparison not only of the mean but also of the variation. The error bar for OMI in this plot only includes the uncertainty of the average of OMI retrievals (assuming accurate AMFs). Other sources of errors,

Water vapor retrieval from OMI visible spectra

H. Wang et al.

Title Page

Abstract | Introduction

Conclusions | References

Tables | Figures

◄ | ►►

◄ | ►

Back | Close

Full Screen / Esc

Printer-friendly Version

Interactive Discussion

including the error of AMFs, the mismatch in timing between OMI and AERONET observations, the difference in observational footprint size, the spread due to scene inhomogeneities and the imperfection of the de-stripping procedure, are not included. Consequently, the total error for OMI should be larger than shown in the figure. Despite
5 of these, we have found reasonably good matches between the two datasets. A few examples are shown in Fig. 7a–f. In these cases, OMI result tracks both the mean and the variation of AERONET result well except for occasional outliers. It is not surprising that we have also found examples where OMI does not agree with AERONET due to the multiple error sources mentioned above. Two examples with large discrepancies
10 are shown in Fig. 7g and h. For Mauna Loa (Fig. 7g), the large difference is partly related to AERONET measurements being on the mountain.

5 Summary

Water vapor is an important molecule for atmospheric weather, climate and chemistry. There are distinct water vapor features in the OMI visible spectra that can be exploited
15 to retrieval water vapor column amount.

In this paper, we have presented our two-step operational OMI water vapor retrieval algorithm. We perform direct spectral fitting in the optimized spectral region 430–480 nm to retrieve water vapor slant column density. This 50 nm-long window includes the water vapor absorption feature at ~ 442 nm and ~ 470 nm. Besides water
20 vapor, we also fit O_3, O_2–O_2, NO_2, liquid water, the Ring effect, the water Ring effect and third order closure polynomials. Our median retrieval uncertainty is about $\sim 1.3 \times 10^{23}$ molecule cm^{-2}, much smaller than that using shorter and narrower retrieval windows. We have examined the sensitivity of our results to the retrieval window, interfering molecules, reference spectra and other factors. Results show that it is important
25 to include liquid water in our standard retrieval and use a relatively long retrieval window to reduce uncertainty.

We convert the slant column densities to vertical column densities using the air mass factors (AMFs). AMFs can be expressed as the integral of the product of the scattering weight and shape factor. In our operational retrieval, we use pre-calculated table for the scattering weight and monthly mean water vapor profiles from GEOS-5 data assimilation product for the shape factor. Our level 2 product contains both averaging kernels and the shape factor for evaluation with and assimilation into models.

We compare our results with the MODIS near-IR and AERONET data. Results show general agreement in terms of the spatial and temporal distribution both at the global level and for many sites. Future work will be concentrated on further refining the retrievals, maintaining the long-term stability and performing extensive data validation.

References

Acarreta, J. R., De Haan, J. F., and Stammes, P.: Cloud pressure retrieval using the O_2–O_2 absorption band at 477,nm, J. Geophys. Res., 109, D05204, doi:10.1029/2003JD003915, 2004.

Aumann, H. H., Chahine, M. T., Gautier, C., Goldberg, M. D., Kalnay, E., McMillin, L. M., Revercomb, H., Rosenkranz, P. W., Smith, W. L., Staelin, D. H., Strow, L. L., and Susskind, J.: AIRS/AMSU/HSB on the Aqua mission: design, science objectives, data products, and processing systems, IEEE T. Geosci. Remote, 41, 253–264, 2003.

Boukabara, S. A., Garrett, K., Chen, W. C.: Global coverage of total precipitable water using a microwave variational algorithm, IEEE T. Geosci. Remote, 48, 10, 3608–3621, doi:10.1109/TGRS.2010.2048035, 2010.

Brion, J., Chakir, A., Daumont, D., Malicet, J., Parisse, C.: High-resolution laboratory absorption cross-section of O_3 – temperature effect, Chem. Phys. Lett., 213, 610–612, doi:10.1016/0009-2614(93)89169-I, 1993.

Caspar, C. and Chance, K. V.: GOME wavelength calibration using solar and atmospheric spectra, in: Third ERS Symposium on Space at the Service of our Environment, edited by Guyenne, T. D. and Danesy, D., vol. 414 of ESA Special Publication, 609 pp., 1997.

Chance, K. V.: Analysis of BrO measurements from the Global Ozone Monitoring Experiment, Geophys. Res. Lett., 25, 3335–3338, 1998.

Chance, K. V. and Kurucz, R. L.: An improved high-resolution solar reference spectrum for Erath's atmosphere measurements in the ultraviolet, visible, and near infrared, J. Quant. Spectr. Radiat. Tran., 111, 1289–1295, doi:10.1016/j.jqsrt.2010.01.036, 2010.

Chance, K. V. and Spurr, R. J. D.: Ring effect studies: Rayleigh scattering, including molecular parameters for rotational Raman scattering, and the Fraunhofer spectrum, Appl. Optics, 36, 5224–5230, 1997.

Chance, K. V., Kurosu, T. P., and Sioris, C. E.: Undersampling correction for array detector-based satellite spectrometers, Appl. Optics, 44, 1296–1304, 2005.

Dirksen, R., Dobber, M., Voors, R., and Levelt, P.: Prelaunch characterization of the Ozone Monitoring Instrument transfer function in the spectral domain, Appl. Optics, 45, 3972–3981, 2006.

Ferraro, R. R., Weng, F. Z., Grody, N. C., Zhao, L. M., Meng, H., Kongoli, C., Pellegrino, P., Qiu, S., Dean, C.: NOAA operational hydrological products derived from the advanced microwave sounding unit, IEEE T. Geosci. Remote, 43, 1036–1049, doi:10.1109/TGRS.2004.843249, 2005.

Gao, B. and Kaufman, Y. J.: Water vapor retrievals using Moderate Resolution Imaging Spectroradiometer (MODIS) near-infrared channels, J. Geophys. Res., 108, 4389, doi:10.1029/2002JD003023, 2003.

González Abad, G., Liu, X., Chance, K., Wang, H., Kurosu, T. P., and Suleiman, R.: Updated SAO OMI formaldehyde retrieval, Atmos. Meas. Tech. Discuss., 7, 1–31, doi:10.5194/amtd-7-1-2014, 2014.

Holben, B. N., Eck, T. F., Slutsker, I., Tanré, D., Buis, J. P., Setzer, A., Vermote, E., Reagan, J. A., Kaufman, Y., Nakajima, T., Lavenu, F., Jankowiak, I., and Smirnov, A.: AERONET – a federated instrument network and data archive for aerosol characterization, Remote Sens. Environ., 66, 1–16, 1998.

King, M., Menzel, W. P., Kaufman, Y. J., Tanre, D., Gao, B. C., Plantnick, S., Ackerman, S. A., Remer, L. A., Pincus, R., Hubanks, P. A.: Cloud and aerosol properties, precipitable water,

and profiles of temperature and water vapor from MODIS, IEEE T. Geosci. Remote, 41, 442–458, doi:10.1109/TGRS.2002.808226, 2003.

Levelt, P. F., van den Oord, G. H. J., Dobber, M. R., Malkki, A., Visser, H., de Vries, J., Stammes, P., Lundell, J. O. V., and Saari, H.: The Ozone Monitoring Instrument, IEEE T. Geosci. Remote, 44, 1093–1101, 2006.

Lindström, P. and Wedin, P.-Å.: Methods and software for nonlinear least squares problems, Technical Report UMINF-133.87, Institute of Information Processing, University of Umeå, Umeå, Sweden, 1988.

Martin, R. V., Chance, K., Jacob, D. J., Kurosu, T. P., Spurr, R. J. D., Bucsela, E., Gleason, J. F., Palmer, P. I., Bey, I., Fiore, A. M., Li, Q., Yantosca, R. M., and Koelemeijer, R. B. A.: An improved retrieval of tropospheric nitrogen dioxide from GOME, J. Geophys. Res., 107, 4437, doi:10.1029/2001JD001027, 2002.

Noel, S., Buchwitz, M., Bovensmann, H., and Burrows, J. P.: Retrieval of total water vapor column amounts from GOME/ERS-2 data, Adv. Space Res., 29, 1697–1702, 2002.

Noël, S., Buchwitz, M., and Burrows, J. P.: First retrieval of global water vapour column amounts from SCIAMACHY measurements, Atmos. Chem. Phys., 4, 111–125, doi:10.5194/acp-4-111-2004, 2004.

Palmer, P. I., Jacob, D. J., Chance, K. V., Martin, R. V., Spurr, R. J. D., Kurosu, T. P., Bey, I., Yantosca, R., Fiore, A., and Li, Q.: Air mass factor formulation for spectroscopic measurements from satellites: application to formaldehyde retrievals from the Global Ozone Monitoring Experiment, J. Geophys. Res., 106, 14539–14550, doi:10.1029/2000JD900772, 2001.

Pope, R. M. and Fry, E. S.: Absorption spectrum (380–700, nm) of pure water. 2. Integrating cavity measurements, Appl. Optics, 36, 8710–8723, doi:10.1364/AO.36.008710, 1997.

Press, W. H., Flannery, T. S., and Vetterling, W. T.: Numerical Recipes: the Art of Scientific Computing, Cambridge Univ. Press, New York, 1986.

Rothman, L. S., Gordon, I. E., Barbe, A., Benner, D. C., Bernath, P. F., Birk, M., Boudon, V., Brown, L. R., Campargue, A., Champion, J.-P., Chance, K., Coudert, L. H., Dana, V., Devi, V. M., Fally, S., Flaud, J. M., Gamache, R. R., Goldman, A., Jacquemart, D., Lacome, N., Lafferty, W. J., Mandin, J. Y., Massie, S. T., Mikhailenko, S. N., Miller, C. E., Moazzen-Ahmadi, N., Naumenko, O. V., Nikitin, A. V., Orphal, J., Perevalov, V. I., Perrin, A., Predoi-Cross, A., Rinsland, C. P., Rotger, M., Simeckova, M., Smith, M. A. H., Sung, K., Tashkun, S. A., Tennyson, J., Toth, R. A., Vandaele, A. C., and Vander Auwera, J.: The HITRAN 2008 molecular spectroscopic database, J. Quant. Spectr. Radiat. Tran., 110, 533–572, 2009.

Rothman, L. S., Gordon, I. E., Babikov, Y., Barbe, A., Benner, D. C., Bernath, P. F., Birk, M., Bizzocchi, L., Boudon, V., Brown, L. R., Campargue, A., Chance, K., Cohen, E. A., Coudert, L. H., Devi, V. M., Drouin, B. J., Fayt, A., Flaud, J. M., Gamache, R. R., Harrison, J. J., Hartmann, J. M., Hill, C., Hodges, J. T., Jacquemart, D., Jolly, A., Lamouroux, J., Le Roy, R. J., Li, G., Long, D. A., Lyulin, O. M., Mackie, C. J., Massie, S. T., Mikhailenko, S., Muller, H. S. P., Naumenko, O. V., Nikitin, A. V., Orphal, J., Perevalov, V., Perrin, A., Polovtseva, E. R., Richard, C., Smith, M. A. H., Starikova, E., Sung, K., Tashkun, S., Tennyson, J., Toon, G. C., Tyuterev, V. G., and Wagner, G.: The HITRAN 2012 molecular spectroscopic database, J. Quant. Spectr. Radiat. Tran., 130, 4–50, 2013.

Schneider, M. and Hase, F.: Optimal estimation of tropospheric H_2O and δD with IASI/METOP, Atmos. Chem. Phys., 11, 11207–11220, doi:10.5194/acp-11-11207-2011, 2011.

Schoeberl, M. R., Douglass, A. R., Hilsenrath, E., Bhartia, P. K., Beer, R., Waters, J. W., Gunson, M. R., Froidevaux, L., Gille, J. C., Barnett, J. J., Levelt, P. F., and de Cola, P.: Overview of the EOS Aura mission, IEEE T. Geosci. Remote, 44, 1066–1074, 2006.

Spurr, R. J. D.: VLIDORT: a linearized pseudo-spherical vector discrete ordinate radiative transfer code for forward model and retrieval studies in multilayer multiple scattering media, J. Quant. Spectr. Radiat. Tran., 102, 316–342, doi:10.1016/j.jqsrt.2006.05.005, 2006.

Stammes, P. and Noordhoek, R.: OMI Algorithm Theoretical Basis Document, vol. III, Clouds, aerosols, and surface UV irradiance, ATBD-OMI-03, Version 2.0, August, 2002.

Stammes, P., Sneep, M., de Haan, J. F., Veefkind, J. P., Wang, P., and Levelt, P. F.: Effective cloud fractions from the Ozone Monitoring Instrument: theoretical framework and validation, J. Geophys. Res., 113, D16S38, doi:10.1029/2007JD008820, 2008.

Thalman, R. and Volkamer, R.: Temperature dependent absorption cross-sections of O_2–O_2 collision pairs between 340 and 630 nm and at atmospherically relevant pressure, Phys. Chem. Chem. Phys., 15, 15371–15381, doi:10.1039/c3cp50968k, 2013.

Veihelmann, B. and Kleipool, Q.: Reducing along-track stripes in OMI-Level 2 products, available at: http://disc.sci.gsfc.nasa.gov/Aura/data-holdings/OMI/documents/v003/RD08_TN785_i1_Reducing_AlongTrack_Stripes.pdf (last access: 17 January 2014), 2006.

Volkamer, R., Spietz, P., Burrows, J., and Platt, U.: High-resolution absorption cross-section of glyoxal in the UV/vis and IR spectral ranges, J. Photochem. Photobio., 172, 35–46, doi:10.1016/j.jphotochem.2004.11.011, 2005.

Water vapor retrieval from OMI visible spectra

H. Wang et al.

Title Page

Abstract | Introduction

Conclusions | References

Tables | Figures

|◀ | ▶|

◀ | ▶

Back | Close

Full Screen / Esc

Printer-friendly Version

Interactive Discussion

Wagner, T., Heland, J., Zöger, M., and Platt, U.: A fast H_2O total column density product from GOME – validation with in-situ aircraft measurements, Atmos. Chem. Phys., 3, 651–663, doi:10.5194/acp-3-651-2003, 2003.

Wagner, T., Beirle, S., Sihler, H., and Mies, K.: A feasibility study for the retrieval of the total column precipitable water vapour from satellite observations in the blue spectral range, Atmos. Meas. Tech., 6, 2593–2605, doi:10.5194/amt-6-2593-2013, 2013.

Worden, J., Kulawik, S., Frankenberg, C., Payne, V., Bowman, K., Cady-Peirara, K., Wecht, K., Lee, J.-E., and Noone, D.: Profiles of CH_4, HDO, H_2O, and N_2O with improved lower tropospheric vertical resolution from Aura TES radiances, Atmos. Meas. Tech., 5, 397–411, doi:10.5194/amt-5-397-2012, 2012.

Water vapor retrieval from OMI visible spectra

H. Wang et al.

Title Page

Abstract | Introduction

Conclusions | References

Tables | Figures

|◄ | ►|

◄ | ►

Back | Close

Full Screen / Esc

Printer-friendly Version

Interactive Discussion

Table 1. Reference Spectrum used in standard retrieval.

Molecule	T (K)	Reference
Water Vapor (H_2O)	280	Rothman et al. (2009)
Ozone (O_3)	228	Brion et al. (1993)
Nitrogen dioxide (NO_2)	220	Vandaele et al. (1998)
Oxygen dimer (O_2–O_2)	294	http://spectrolab.aeronomie.be/o2.htm
Pure Liquid water (H_2O)	–	Pope and Fry (1997)
Glyoxal ($C_2H_2O_2$)	296	Volkamer et al. (2005)
Ring and Water Ring	–	Chance and Spurr (1997)

Title Page

Abstract | Introduction

Conclusions | References

Tables | Figures

|◄ | ►|

◄ | ►

Back | Close

Full Screen / Esc

Printer-friendly Version

Interactive Discussion

Table 2. Sensitivity to retrieval window.

Window Length (nm)	Retrieval Window (nm)	Median SCD (molecule cm^{-2})	Median Uncertainty (molecule cm^{-2})	Median Relative Uncertainty
20	[435, 455]	1.47×10^{23}	2.4×10^{22}	0.19
30	[432, 462]	1.43×10^{23}	2.0×10^{22}	0.17
40	[438, 478]	1.35×10^{23}	1.6×10^{22}	0.15
50 (standard)	[430, 480]	1.32×10^{23}	1.2×10^{22}	0.11
65	[430, 495]	1.23×10^{23}	1.5×10^{22}	0.12

Table 3. Miscellaneous sensitivity studies.

Description	Median SCD (molecule cm^{-2})	Median uncertainty (molecule cm^{-2})	Median RMS	Number of negatives
Standard	1.32×10^{23}	1.2×10^{22}	9.2e−4	1935
Without O$_3$	1.19×10^{23}	1.2×10^{22}	9.3e−4	7234
Without O$_2$–O$_2$	1.18×10^{23}	1.3×10^{22}	9.9e−4	5076
Without NO$_2$	1.05×10^{23}	1.2×10^{22}	9.3e−4	15 666
Without liquid water	0.90×10^{23}	1.1×10^{22}	9.5e−4	50 216
Without C$_2$H$_2$O$_2$	1.34×10^{23}	1.2×10^{22}	9.2e−4	1780
Switch to 5th order polynomial	1.32×10^{23}	1.3×10^{22}	9.0e−4	2262
Switch reference H$_2$O to 0.7 atm and 265 K	1.29×10^{23}	1.2×10^{22}	9.2e−4	1992
Switch reference H$_2$O to 1.0 atm and 288 K	1.34×10^{23}	1.2×10^{22}	9.2e−4	1918
Switch to Rothman et al. (2013) HITRAN 2012 water vapor	1.24×10^{23}	1.2×10^{22}	9.2e−4	1816
Switch to Thalman et al. (2013) O$_2$–O$_2$	1.31×10^{23}	1.2×10^{22}	9.2e−4	2185
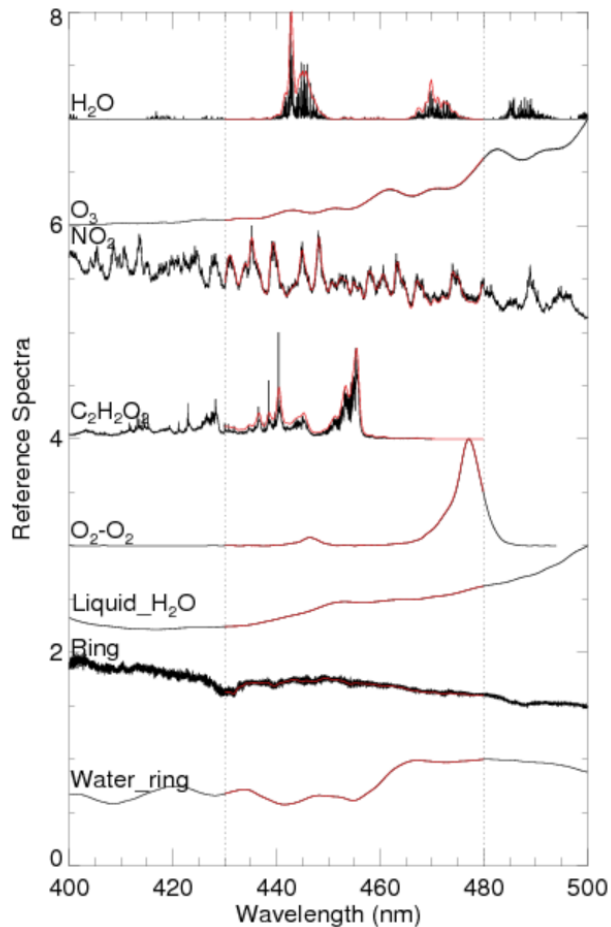
Fig. 1. Reference spectra used in the standard operational water vapor retrieval. The spectra have been scaled for presentation. Black lines are those listed in Table 1. Red lines are the black lines convolved with the OMI slit function.
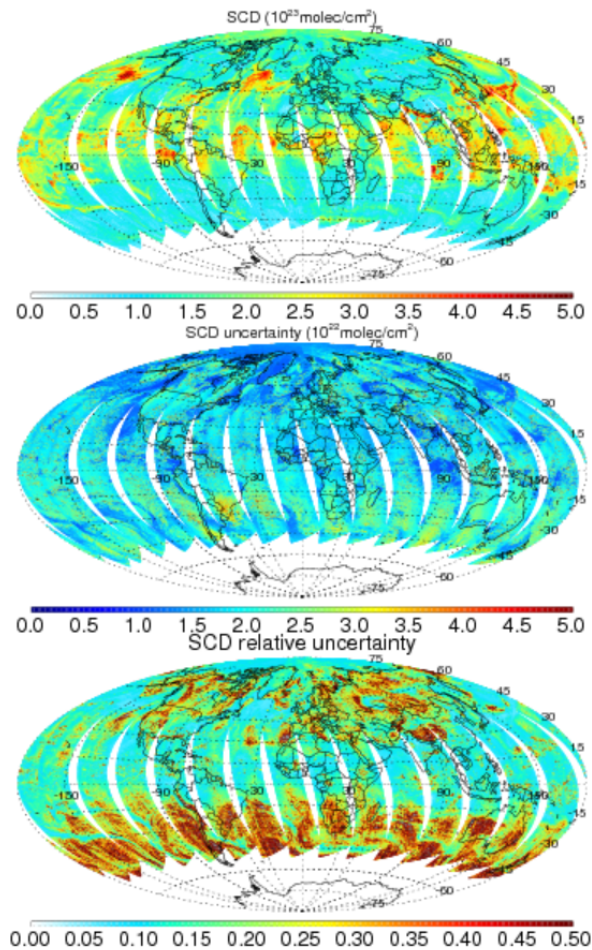
Fig. 2. OMI water vapor (top) SCD, (middle) SCD uncertainty, and (bottom) SCD relative uncertainty on 14 July 2005 from our standard retrieval.
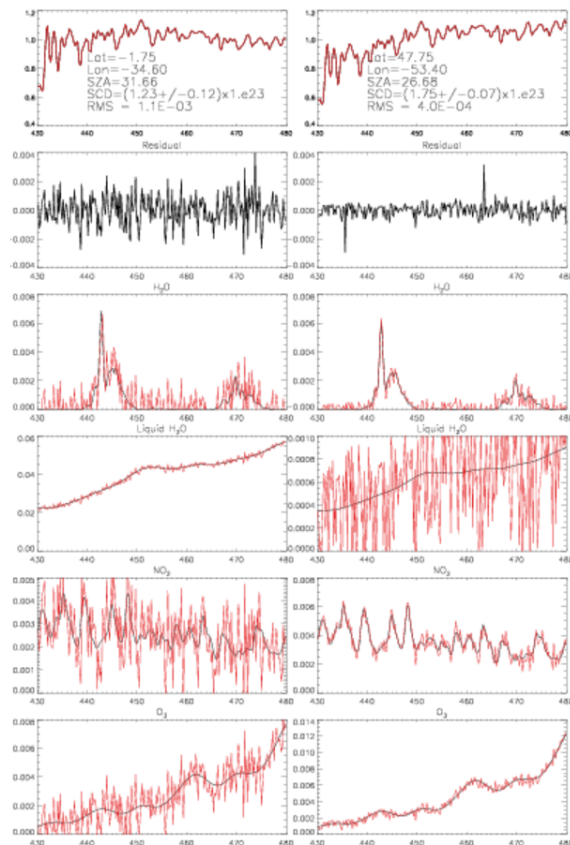
Fig. 3. Spectral fitting for a pixel in the Atlantic ocean (left) and a pixel near the Atlantic coast of North America (right). The 1st row shows the fitted (red) spectra overplotted on the measured (black) spectra. The 2nd row shows the fitting residuals. The 3rd–6th rows show the reference spectra of H_2O, liquid H_2O, NO_2 and O_3 scaled by the fitted slant columns (black) and added to the fitting residuals (red).
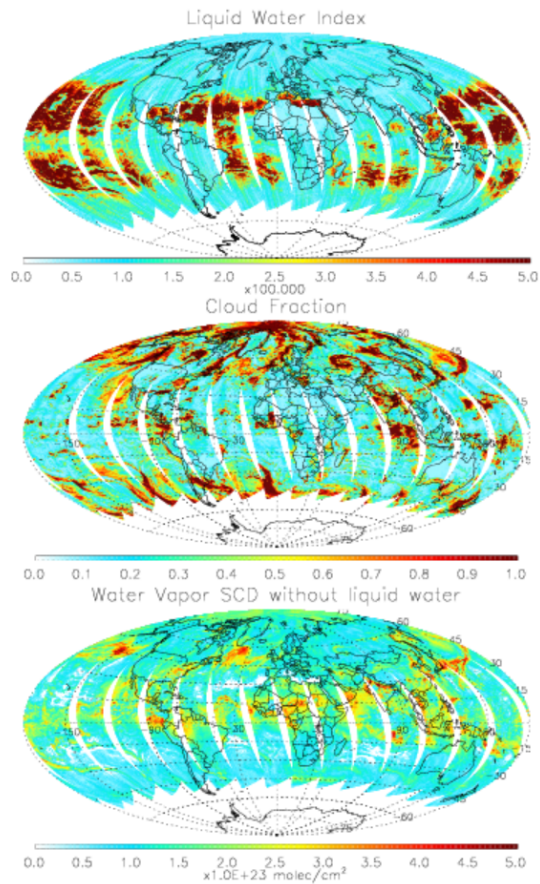
Fig. 4. Top panel shows the by-product of liquid water index from our standard water vapor retrieval. Middle panel shows the cloud fraction from the OMI cloud product used in our retrieval. Bottom panel shows the water vapor SCD from a sensitivity study where liquid water is excluded from the water vapor retrieval. All results are for 14 July 2005.
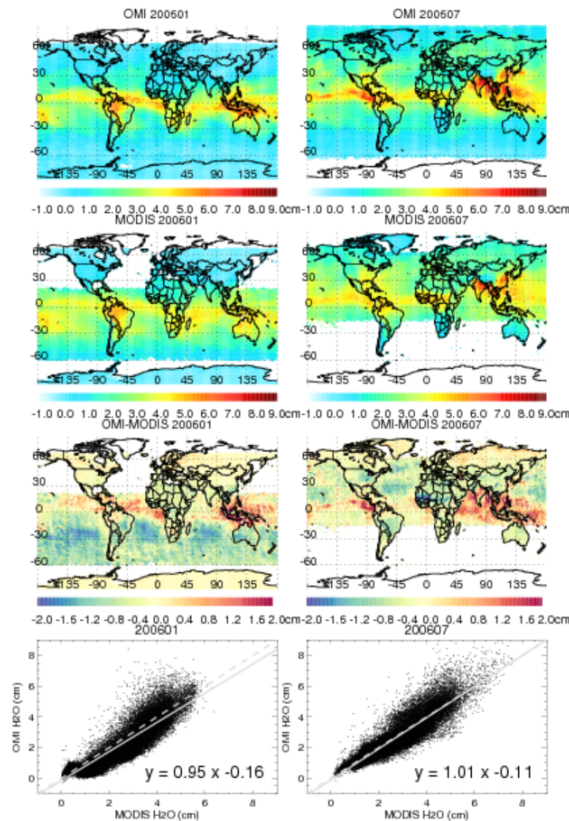
Fig. 5. Top row shows the monthly mean OMI total precipitable water (cm) gridded to 1°
longitude ×1° latitude for January and July 2006 derived from our standard retrieval. Second
row shows the corresponding MODIS near-IR precipitable water (cm). Third row shows the
OMI – MODIS difference (cm). Bottom row shows the scatter plots of MODIS vs. OMI results.
The 1 : 1 line is indicated by the gray dashed line in each panel. The regression line represented
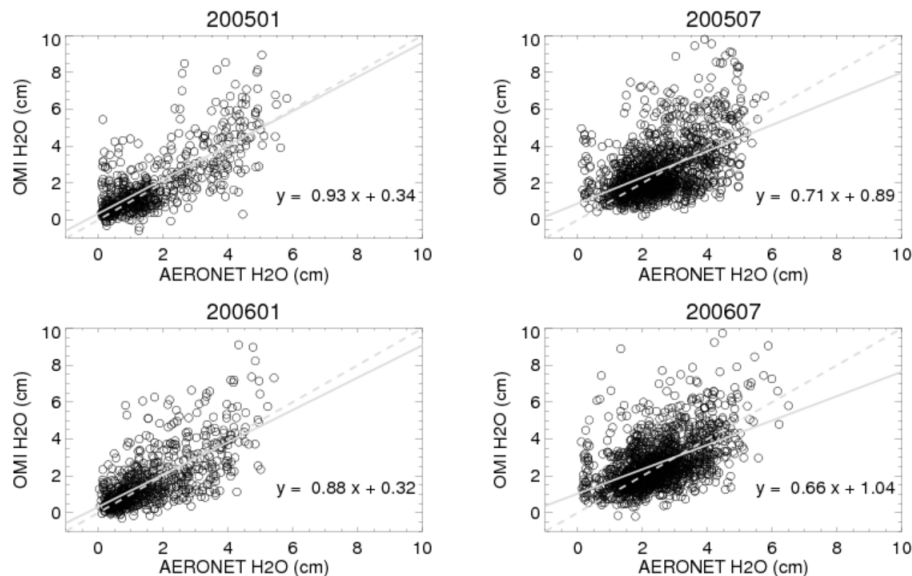by the equation in each panel is indicated by the gray solid line.

Fig. 6. Scatter plots of AERONET vs. OMI precipitable water (cm) for (top left) January 2005, (top right) July 2005, (bottom left) January 2006, and (bottom right) July 2006. The regression lines indicated in the plot are shown by the gray solid lines. The 1 : 1 lines are shown by the gray dashed lines.
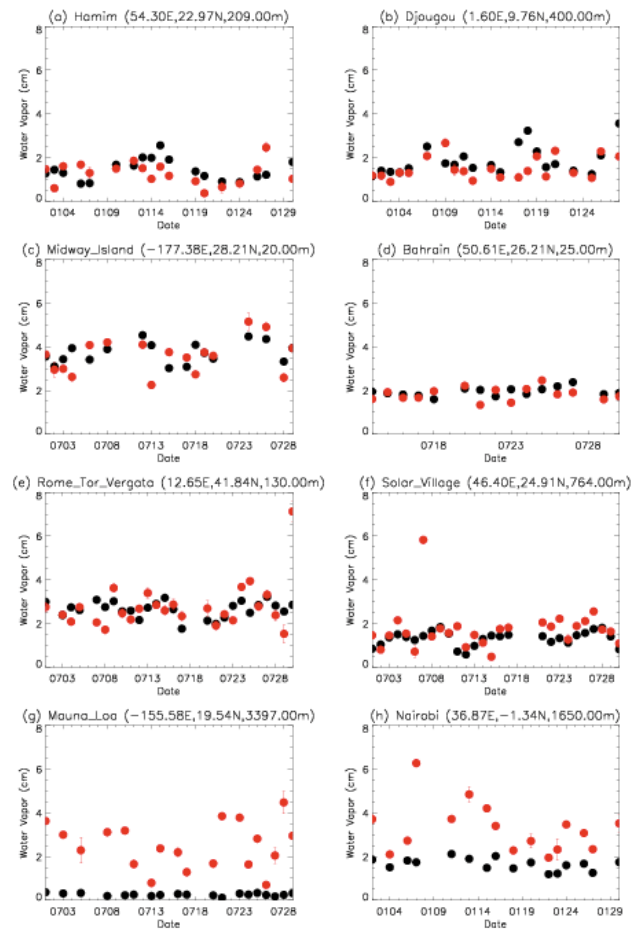
Fig. 7. Time series comparisons between AERONET (black) and OMI (red) precipitable water (cm) at selected AERONET sites in 2006. Date is indicated by month and day.